TiS Trends in Sciences
TRENDS IN SCIENCES 2027; 24(2): 14543
SPRINT Scholarly Publishing and Repository Integration Center
https://doi.org/10.48048/tis.2027.14543
RESEARCH ARTICLE

Evaluation of ASHB-5 and ASHB-6 Complexes as Novel Anti-Inflammatory Candidates Using Carrageenan-Induced Paw Edema and Molecular Docking Approaches

Dadamirzayeva Kamola[1*], Bakiyeva Muazzam[2], Najimov Akmaljon[2], Rezhepov Kural Zhedgerovich[3], Shiyrin Bekniyaz Kizi Alimbayeva[3] and Bekniyaz Alimbayevich Khodzhaniyazov[4]

[1]*Department of Medicine, Tashkent International University of Chemistry, Namangan Branch, Namangan, Uzbekistan*
[2]*Department of Medicine, Namangan State University, Namangan, Uzbekistan*
[3]*Laboratory of "Small Molecular Biologically Active Compounds" Institute of Bioorganic Chemistry named after A.S. Sadykov Academy of Sciences of the Republic of Uzbekistan, Tashkent, Uzbekistan*
[4]*Department of Chemical Technology, Karakalpak State University named after Berdakh, Nukus, Uzbekistan*

([*]Corresponding author's e-mail: kamoladadamirzayeva13041985@gmail.ru)

Received: 30 May 2026, Revised: 25 June 2026, Accepted: 6 July 2026, Published: 1 October 2026

Abstract

Inflammation is a complex biological response regulated by multiple mediators, enzymes, cytokines, and intracellular signaling pathways. The present study aimed to evaluate the anti-inflammatory potential of ASHB-5 and ASHB-6 complexes using an integrated *in vivo* and *in silico* approach. The anti-exudative activity of the complexes was investigated in rats using the carrageenan-induced paw edema model. ASHB-5 and ASHB-6 were administered orally at doses of 12.5 and 25 mg/kg, and paw edema development was monitored after carrageenan injection. Molecular docking analysis was performed against key inflammation-related targets, including cyclooxygenase-2 (COX-2), interleukin-6 (IL-6), mitogen-activated protein kinase (MAPK), and nuclear factor-kappa B (NF-kB), to explore possible molecular mechanisms underlying the observed effects. *In vivo* results showed that both ASHB-5 and ASHB-6 reduced carrageenan-induced paw edema in a dose-dependent manner. At 12.5 mg/kg, ASHB-5 demonstrated stronger anti-exudative activity than ASHB-6, with inhibition values of 42.9 ± 5.1% and 28.4 ± 3.7%, respectively. At 25 mg/kg, ASHB-6 produced the most pronounced effect, reaching 64.6 ± 4.8% inhibition, whereas ASHB-5 showed 52.1 ± 4.6% activity. These findings indicate that ASHB-5 was more effective at the lower dose, while ASHB-6 exhibited greater activity at the higher dose. Docking analysis revealed favorable predicted interactions of both complexes with COX-2, IL-6, MAPK, and NF-kB. Particularly strong binding profiles were observed for COX-2 and NF-kB, especially for ASHB-6, which showed the strongest predicted interaction with NF-kB. Overall, the combined *in vivo* and *in silico* findings suggest that ASHB-5 and ASHB-6 may exert anti-inflammatory effects through multi-target mechanisms involving prostaglandin-mediated inflammation, cytokine-related signaling, MAPK-associated intracellular pathways, and NF-kB-mediated transcriptional regulation. These results support further pharmacological investigation of ASHB-5 and ASHB-6 as potential multi-target anti-inflammatory candidates.

Keywords: ASHB complexes, Anti-inflammatory activity, Carrageenan-induced paw edema, Anti-exudative activity, Molecular docking, COX-2, NF-kB

Introduction

Inflammation represents a highly coordinated biological defense response that occurs after tissue injury, infection, or exposure to harmful chemical and physical stimuli. Under physiological conditions, acute inflammation plays a beneficial role by removing injurious agents, limiting tissue damage, and initiating repair processes. However, when inflammatory

responses become excessive, uncontrolled, or prolonged, they may contribute to the pathogenesis of numerous diseases, including arthritis, cardiovascular complications, metabolic disorders, neurodegenerative conditions, and chronic tissue injury. Therefore, the identification of novel anti-inflammatory compounds with favorable efficacy, reduced toxicity, and the ability to affect multiple inflammatory pathways remains a relevant priority in pharmacological and biomedical research. The development and progression of inflammation are controlled by multiple interconnected mediators, enzymes, cytokines, and intracellular signaling cascades. Cyclooxygenase-2 (COX-2), interleukin-6 (IL-6), mitogen-activated protein kinases (MAPKs), and nuclear factor-kappa B (NF-kB) are among the key molecular regulators involved in inflammatory reactions. COX-2 contributes to the formation of prostaglandins, which are closely associated with pain, edema formation, and increased vascular permeability. IL-6 is an important pro-inflammatory cytokine that participates in immune cell activation, acute-phase responses, and the continuation of inflammatory signaling. In addition, NF-kB and MAPK signaling pathways regulate the transcription of many inflammation-related genes and coordinate cellular responses to inflammatory stimuli. Accordingly, compounds capable of modulating these targets may provide meaningful therapeutic potential against inflammatory disorders. The carrageenan-induced paw edema model is a well-established and widely applied experimental method for screening the anti-inflammatory properties of bioactive substances. This model produces a reproducible acute inflammatory response and enables the evaluation of different phases of edema development. The initial phase is mainly mediated by histamine, serotonin, and bradykinin release, while the later phase is predominantly associated with prostaglandin synthesis, COX-2 activity, and cytokine-dependent inflammatory mechanisms. Therefore, this model is particularly useful for assessing compounds that may suppress mediator-driven inflammatory processes. Alongside experimental pharmacology, molecular docking has become a valuable computational tool for exploring the possible mechanisms of action of biologically active compounds. Docking analysis allows prediction of ligand–protein binding affinity, interaction patterns, and the amino acid residues involved in ligand stabilization within the active or functional regions of target proteins. When interpreted together with *in vivo* findings, molecular docking can strengthen mechanistic understanding and help explain whether the observed pharmacological effects may be related to interactions with inflammation-associated molecular targets. ASHB-5 and ASHB-6 are complex compounds that may possess pharmacological activity; however, their anti-inflammatory effects and underlying molecular mechanisms remain insufficiently investigated. Considering the multi-component and multi-target nature of inflammatory responses, the combined use of *in vivo* and *in silico* approaches may provide a more comprehensive evaluation of these compounds. Therefore, the present study aimed to assess the anti-inflammatory activity of ASHB-5 and ASHB-6 complexes using the carrageenan-induced paw edema model and to investigate their potential interactions with major inflammation-related targets, including COX-2, IL-6, MAPK, and NF-kB, through molecular docking analysis.

Materials and methods

Preparation and composition of the supramolecular complexes

Glycyrrhiza glabra L. belongs to the Fabaceae family and is one of the medicinal plants widely distributed in Uzbekistan. Glycyrrhizic acid was isolated from the roots of locally collected *G. glabra*, and its monoammonium salt was subsequently prepared. Water-soluble supramolecular complexes were obtained by modification of glycyrrhizic acid monoammonium salt with Schiff-base derivatives of β-hydroxy-α-naphthaldehyde at a molar ratio of 12:1. The resulting supramolecular complexes were conditionally designated according to the corresponding Schiff-base derivative. The complete complexes were used in the *in vivo* experiments. In the molecular docking study, the monoammonium salt of glycyrrhizic acid and the corresponding Schiff-base component were docked separately. This approach was used because the applied docking software evaluates discrete molecular structures and does not adequately simulate the dynamic association of an intact supramolecular complex.

Evaluation of anti-exudative activity in carrageenan-induced paw edema in rats

The anti-inflammatory effects of ASHB-5 and ASHB-6 were assessed in rats using the well-established carrageenan-induced hind paw edema model. Same-sex rats weighing 190 ± 20 g were used in the experiment and divided into control and treatment groups, with 4 animals in each group [6]. Acute paw inflammation was induced by subplantar injection of 0.1 mL of 1% carrageenan solution into the hind paw. The test compounds, ASHB-5 and ASHB-6, were given orally at doses of 12.5 and 25 mg/kg 1 h before carrageenan administration. Control rats received the appropriate vehicle in the same manner. Paw edema development was monitored by recording paw volume changes at 1, 2, 3, and 4 h following carrageenan injection. Anti-exudative activity was determined using the edema values measured at the 3rd h, as this interval corresponded to the maximum inflammatory response observed in the control animals. The inhibitory effect of each compound was expressed as a percentage relative to the untreated control group and calculated using the following equation:

$$Anti-exudative\ activity\ (\%) = \frac{Vc-Vt}{Vc} \times 100$$

where Vc indicates the increase in paw volume in the control group, and Vt indicates the increase in paw volume in the treated group [7].

Animal ethics

All experimental procedures involving animals were reviewed and approved by the Animal Ethics Committee of the Institute of Bioorganic Chemistry, Academy of Sciences of the Republic of Uzbekistan prior to the initiation of the study (Protocol No. 133/1a/h, dated August 4, 2014). The animals were maintained under standard vivarium conditions at a controlled temperature of 22 ± 2 °C and relative humidity of 55% - 65%, with free access to drinking water and a standard laboratory diet. Animal care, handling, and experimental procedures were carried out in accordance with the principles of humane animal use and complied with European Directive 2010/63/EU for the protection of animals used for scientific purposes.

Computational tools and databases

All computational analyses were performed using freely available academic research tools and structural bioinformatics resources. The 3-dimensional structures of the selected inflammation-related target proteins were obtained from the Protein Data Bank (PDB), a widely recognized database of experimentally determined biological macromolecular structures [8]. Based on their important roles in inflammatory pathways, 4 target proteins were selected for molecular docking analysis: cyclooxygenase-2 (COX-2, PDB ID: 5IKR), interleukin-6 (IL-6, PDB ID: 1ALU), mitogen-activated protein kinase (MAPK, PDB ID: 2OJJ), and nuclear factor-kappa B (NF-kB, PDB ID: 1LE9). For the NF-kB target, the p50/p65 heterodimer complex bound to DNA was retrieved from the PDB using the structure ID 1LE9. Prior to docking simulations, the DNA molecule was removed from the complex, and only the remaining NF-kB protein structure was retained as the receptor [9]. The prepared NF-kB protein was then used for docking analysis with ASHB-5 and ASHB-6. The molecular structures of ASHB-5 and ASHB-6 were prepared and optimized before docking. All protein structures downloaded in PDB format were initially inspected using PyMOL to verify their structural suitability. During receptor preparation, crystallographic water molecules, irrelevant heteroatoms, and the DNA chain in the NF-kB complex were removed. PyMOL was also used for visualization of the protein structures and for post-docking inspection of ligand–protein interactions. Further preparation of receptors and ligands was performed using AutoDock Tools [9]. This step included the addition of polar hydrogen atoms, assignment of partial charges, definition of rotatable bonds in the ligands, and conversion of the prepared receptor and ligand structures into the required docking format. Molecular docking simulations were carried out using AutoDock 4.2 to identify the most favorable binding conformations of ASHB-5 and ASHB-6 within the active or functionally important regions of the selected inflammatory targets [10]. Docking results were evaluated based on binding free energy values expressed in kcal/mol, as well as the formation of hydrogen bonds, hydrophobic interactions, and other non-covalent contacts between the ligands and target proteins. The resulting molecular interaction profiles were used to support the possible mechanisms

underlying the anti-inflammatory effects of ASHB-5 and ASHB-6 complexes.

Target selection and binding-site rationale

COX-2, IL-6, MAPK, and NF-κB were selected because they represent different components of the inflammatory response. For COX-2 and MAPK, docking was performed within structurally defined ligand-binding regions. For IL-6, the selected region represented a potential small-molecule interaction area associated with the cytokine surface involved in receptor-complex formation. For NF-κB, DNA was removed from the crystallographic complex, and docking was conducted near the functionally relevant DNA-binding/interface region. Unlike COX-2 and MAPK, IL-6 and NF-κB lack well-defined catalytic pockets and contain relatively shallow and flexible protein-interaction surfaces. Consequently, docking results for these proteins were considered exploratory predictions of possible structural compatibility and not evidence of direct inhibition or pathway modulation.

Preparation of ligand and protein files

Prior to molecular docking, all receptor structures obtained from the Protein Data Bank were prepared using a standardized protein preprocessing workflow. Since raw PDB files often contain crystallographic water molecules, co-crystallized ligands, ions, missing hydrogen atoms, and other non-essential heteroatoms, direct use of these structures in docking simulations may affect the accuracy of ligand–receptor interaction predictions [11]. Therefore, each selected inflammatory target, including COX-2, IL-6, MAPK, and NF-kB, was carefully processed before docking analysis. The receptor structures were imported into AutoDock Tools (ADT) for preparation. During this step, crystallographic water molecules, irrelevant heteroatoms, ions, and other non-protein components were removed. Co-crystallized ligands were also deleted from the receptor structures before docking calculations. When necessary, these native ligands were saved separately and used for validation of the docking protocol. For the NF-kB protein–DNA complex, the bound DNA molecule was removed, and only the protein component was retained as the receptor for subsequent docking simulations. This preparation strategy was applied to minimize possible artificial electrostatic effects and to ensure that docking was performed only against the relevant protein target under the rigid receptor approximation. The prepared receptor structures were visually inspected using PyMOL to confirm structural integrity and to identify any missing residues in functionally important regions [12]. No critical missing residues were detected in the selected target proteins that could substantially influence the docking analysis. After visual inspection, polar hydrogen atoms were added to the receptor molecules, and Kollman united atom charges were assigned using AutoDock Tools. Protonation states were prepared according to the standard ADT workflow to approximate physiological conditions at pH 7.4. The final receptor files were saved in .pdbqt format, which includes atom type information and partial charges required for AutoDock-based docking calculations. The ligand structures of ASHB-5 and ASHB-6 were prepared using a similar procedure. Each compound was imported into AutoDock Tools, hydrogen atoms were added, and Gasteiger charges were assigned. Non-polar hydrogen atoms were merged according to the standard AutoDock preparation protocol. Rotatable bonds and root atoms were automatically detected by ADT and manually checked when required to ensure appropriate ligand flexibility during docking. Finally, the optimized ASHB-5 and ASHB-6 ligand structures were exported in .pdbqt format and used for molecular docking simulations against the selected inflammation-related targets [13].

Docking protocol validation

The docking protocol was validated by removing the co-crystallized ligand from the protein structure and redocking it into the original binding site using the same docking parameters applied to the investigated compounds. The predicted ligand pose was superimposed on the crystallographic pose, and the root-mean-square deviation (RMSD) was calculated. An RMSD value below 2.0 Å was considered indicative of acceptable docking performance.

Calculation of inhibition constant (Ki) from binding energy

In molecular docking studies, the strength of ligand–target interaction is usually described by the binding free energy (ΔG), which is reported in kcal/mol

[14]. Along with binding energy, the inhibition constant (Ki) was considered as a theoretical value derived from the calculated ΔG. In docking-based interpretation, Ki serves as an estimated indicator of ligand affinity toward the target protein and may provide additional insight into the predicted inhibitory potential of the compound. Generally, lower Ki values correspond to stronger predicted binding affinity and greater theoretical inhibitory potential, while higher Ki values indicate weaker ligand–protein interaction. Nevertheless, Ki values obtained from docking calculations should be regarded only as computational predictions rather than experimentally determined inhibition constants.

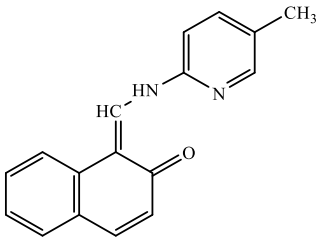
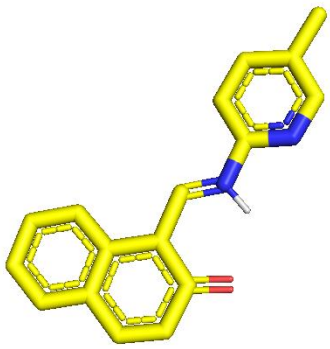
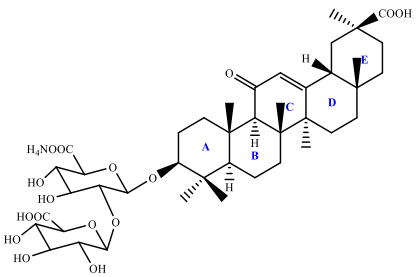
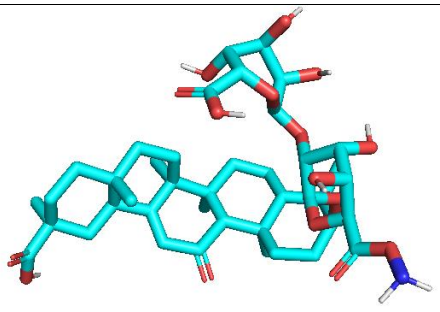
$$Ki = e^{\frac{\Delta G \times 1{,}000}{R \times T}}$$

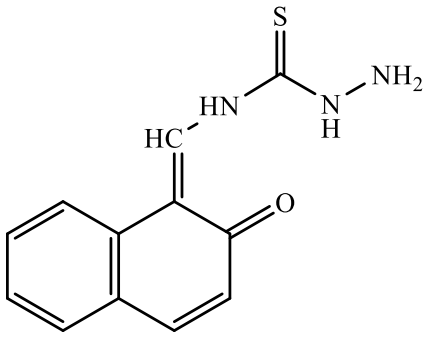
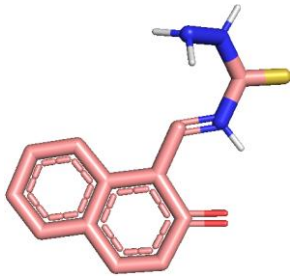
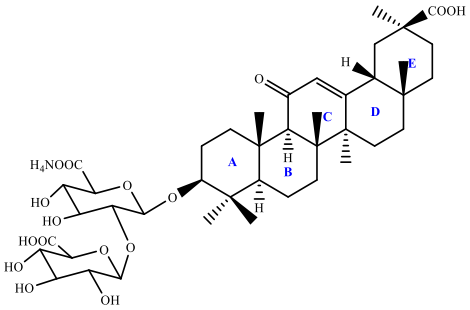
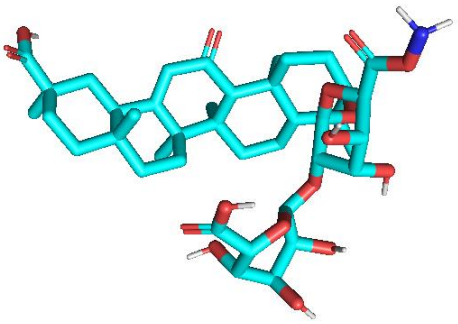
where, Ki is the inhibition constant (in mol/L); ΔG is the binding free energy (in kcal/mol); - R is the universal gas constant = 1.987 cal/(mol·K); T is the temperature in Kelvin (usually 298.15 K); The factor 1,000 converts kcal to cal.

Statistical analysis

Experimental data were analyzed and visualized using OriginPro 9.0 software (OriginLab Corporation, USA). All results are expressed as mean ± standard error of the mean (SEM), with 4 animals included in each experimental group. Since paw edema was measured repeatedly in the same animals at 1, 2, 3, and 4 h following carrageenan administration, the time-course data were analyzed using 2-way repeated-measures analysis of variance. Treatment group was considered the between-subject factor, while time was considered the within-subject factor. The main effects of treatment and time, as well as the treatment×time interaction, were evaluated. Where significant differences were identified, an appropriate post hoc multiple-comparison test was applied to compare the treatment groups with the untreated control group. Differences were considered statistically significant at $p<0.05$. Model assumptions were assessed by examining residual distribution, homogeneity of variance, and the covariance structure of the repeated observations. Exact *p*-values and 95% confidence intervals were reported where available. Statistical significance was defined as $p < 0.05$.

Table 1 Structural representation of ASHB-5 and ASHB-6 complexes prepared for docking simulations.

Ligands	2D	3D
ASHB-5		
		

Ligands	2D	3D
ASHB-6		
		

Results and discussion

Effect of ASHB-5 and ASHB-6 at 12.5 mg/kg on carrageenan-induced paw edema

At a dose of 12.5 mg/kg, ASHB-5 and ASHB-6 both reduced carrageenan-induced acute paw inflammation when compared with the untreated control group. In the control group, the inflammatory response increased in a time-dependent manner during the first 3 h after carrageenan injection. Paw inflammation was 31.7 ± 3.0% at 1 h and 52.8 ± 5.1% at 2 h, reaching its maximum level at the 3rd h with a value of 73.9 ± 7.2% (**Figure 1**). Although the inflammatory response declined at the 4th h, it remained relatively high at 42.2 ± 4.1%, indicating that the carrageenan-induced inflammatory process was still maintained in untreated animals. Treatment with ASHB-5 at 12.5 mg/kg produced a clear reduction in paw edema formation throughout the observation period. In this group, paw inflammation values were 21.1 ± 2.0%, 31.7 ± 3.0%, 42.2 ± 4.2%, and 34.4 ± 3.3% at 1, 2, 3, and 4 h, respectively. The strongest inhibitory effect was observed at the 3rd h, which coincided with the peak inflammatory response in the control group. At this time point, ASHB-5 decreased paw inflammation from 73.9 ± 7.2% to 42.2 ± 4.2%, corresponding to an anti-exudative activity of approximately 42.9%. ASHB-6 administered at the same dose also suppressed carrageenan-induced paw inflammation, but its effect during the peak phase was weaker than that of ASHB-5. The inflammation values recorded in the ASHB-6-treated group were 21.1 ± 2.0%, 42.2 ± 4.2%, 52.9 ± 5.2%, and 31.7 ± 3.1% at 1, 2, 3, and 4 h, respectively. At the 3rd h, ASHB-6 reduced the inflammatory response to 52.9 ± 5.2%, which corresponded to an anti-exudative activity of approximately 28.4% relative to the untreated control group.

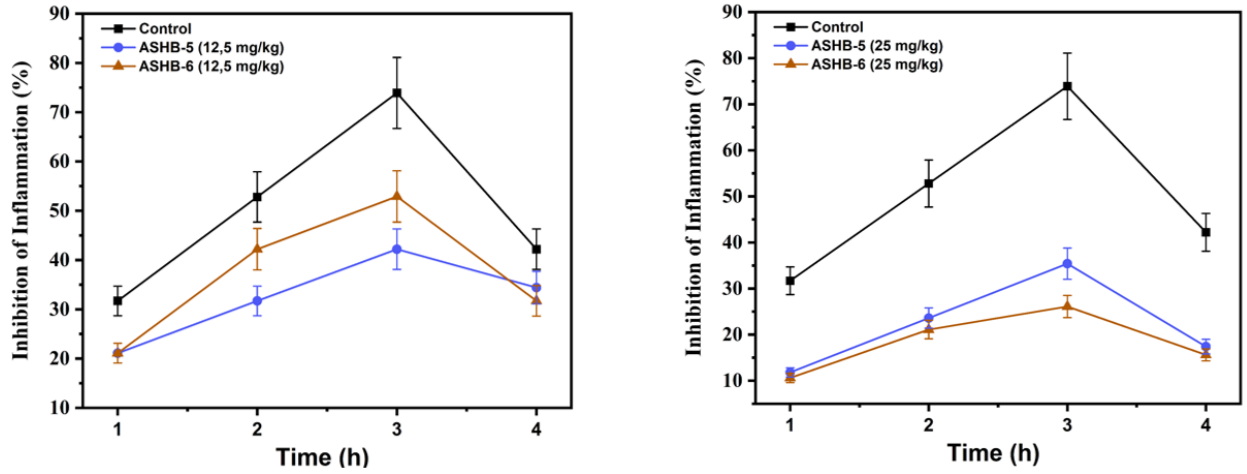


Figure 1 Dose-dependent inhibition of carrageenan-induced paw edema by ASHB-5 and ASHB-6 in rats.

At 25 mg/kg, both ASHB-5 and ASHB-6 caused a marked reduction in carrageenan-induced paw inflammation compared with the untreated control animals. In the control group, inflammation developed progressively during the first 3 h after carrageenan injection and reached its maximum value at the 3rd h, with paw inflammation of 73.9 ± 7.2% (**Figure 1**). Thereafter, the response partially declined to 42.2 ± 4.1% at the 4th h, although inflammation remained evident in the untreated animals. Administration of ASHB-5 at 25 mg/kg substantially suppressed paw edema formation at all investigated time points. The recorded paw inflammation values were 11.8 ± 1.0%, 23.6 ± 2.2%, 35.4 ± 3.4%, and 17.4 ± 1.6% at 1, 2, 3, and 4 h, respectively. The maximal inhibitory effect of ASHB-5 was observed at the 3rd h, which corresponded to the peak inflammatory phase in the control group. At this point, ASHB-5 reduced inflammation from 73.9 ± 7.2% in the control group to 35.4 ± 3.4%, indicating an anti-exudative activity of approximately 52.1%. ASHB-6 demonstrated a stronger anti-inflammatory profile at the same dose. In animals treated with ASHB-6, paw inflammation was 10.6 ± 1.0% at 1 h, 21.1 ± 2.0% at 2 h, 26.1 ± 2.4% at 3 h, and 15.6 ± 1.3% at 4 h. During the peak phase of carrageenan-induced inflammation, ASHB-6 reduced the inflammatory response to 26.1 ± 2.4%, corresponding to an anti-exudative effect of approximately 64.7% relative to the control group.

Dose-dependent anti-exudative effects of ASHB-5 and ASHB-6 at the peak phase of carrageenan-induced paw edema

During the peak stage of carrageenan-induced inflammation, observed at the 3rd h after carrageenan injection, the untreated control animals exhibited a marked elevation in paw edema, reaching 73.9 ± 7.2% (**Figure 2**). Treatment with ASHB-5 at 12.5 mg/kg significantly suppressed edema development, reducing the paw edema value to 42.2 ± 4.1%. This effect corresponded to an anti-exudative activity of approximately 42.9% relative to the control group. ASHB-6 administered at the same dose also significantly decreased paw edema, lowering it to 52.9 ± 5.2%, with an estimated anti-exudative activity of approximately 28.4%. A comparative evaluation indicated that both ASHB-5 and ASHB-6 reduced edema formation during the maximal phase of the inflammatory response. However, ASHB-5 produced a more pronounced anti-exudative effect than ASHB-6 at 12.5 mg/kg, suggesting stronger suppression of acute carrageenan-induced edema under the present experimental conditions.

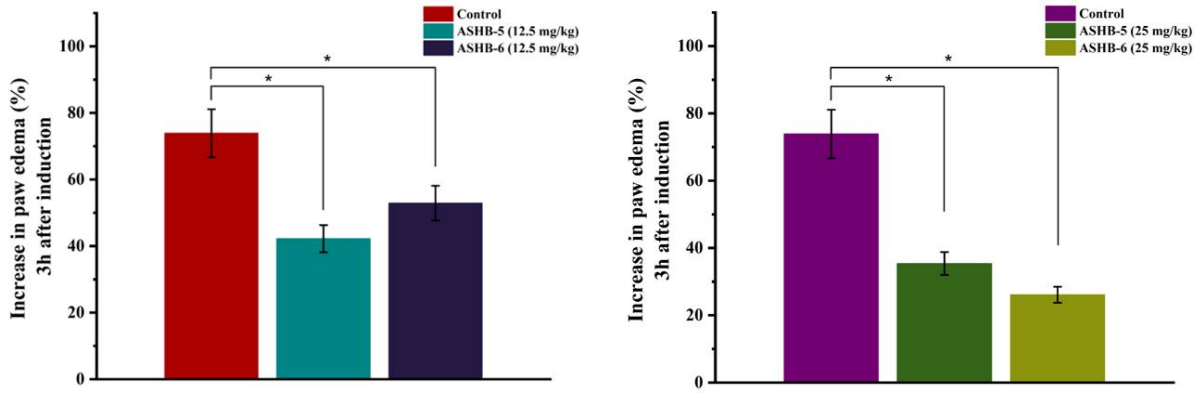


Figure 2 Comparative dose-dependent inhibition of carrageenan-induced paw edema by ASHB-5 and ASHB-6 at the peak inflammatory phase.

A further increase in the administered dose to 25 mg/kg resulted in a stronger suppression of carrageenan-induced paw edema. At the 3rd h after carrageenan injection, which corresponded to the maximal phase of acute inflammation, the untreated control group exhibited a pronounced increase in paw edema, reaching 73.9 ± 7.2% (**Figure 2**). In contrast, treatment with ASHB-5 at 25 mg/kg significantly decreased paw edema to 35.4 ± 3.4%, corresponding to an anti-exudative activity of approximately 52.1% relative to the control group. ASHB-6 at the same dose produced an even more pronounced inhibitory effect, reducing paw edema to 26.1 ± 2.4%, with an estimated anti-exudative activity of approximately 64.7%. Compared with the 12.5 mg/kg dose, both complexes demonstrated enhanced anti-exudative activity at 25 mg/kg, indicating a dose-dependent increase in their anti-inflammatory efficacy. Notably, ASHB-6 showed a stronger effect than ASHB-5 at the higher dose, suggesting a more effective suppression of mediator-dependent edema formation during the peak inflammatory phase. Taken together, these results indicate that both ASHB-5 and ASHB-6 possess significant anti-inflammatory potential, with ASHB-6 displaying the highest activity at 25 mg/kg under the present experimental conditions.

Anti-exudative activity of ASHB-5 and ASHB-6 during the peak phase of carrageenan-induced inflammation

In the carrageenan-induced paw edema model, the inflammatory response typically reaches its highest level during the later stage of acute inflammation, most prominently around the 3rd h after carrageenan injection. This period is mainly associated with the involvement of prostaglandins and cytokine-related inflammatory mediators. Therefore, in the present study, the anti-exudative activity of ASHB-5 and ASHB-6 was assessed using the paw edema values recorded at the 3rd h, when the maximal inflammatory response was observed in the untreated control group. This time point was selected to provide a reliable comparison of the inhibitory effects of both complexes during the most active phase of edema development.

At the lower tested dose of 12.5 mg/kg, both ASHB-5 and ASHB-6 demonstrated measurable anti-exudative activity. ASHB-5 inhibited edema formation by 42.9 ± 5.1% (**Figure 3**), whereas ASHB-6 produced a comparatively weaker effect, with an anti-exudative activity of 28.4 ± 3.7%. These results show that both investigated complexes were capable of reducing carrageenan-induced exudative inflammation even at the lower dose. However, ASHB-5 displayed a stronger inhibitory effect than ASHB-6 at 12.5 mg/kg, indicating greater effectiveness in suppressing edema formation during the peak stage of acute inflammation. This observation is in agreement with the paw edema measurements, where ASHB-5 produced a more pronounced reduction in the inflammatory response at the 3rd h compared with ASHB-6.

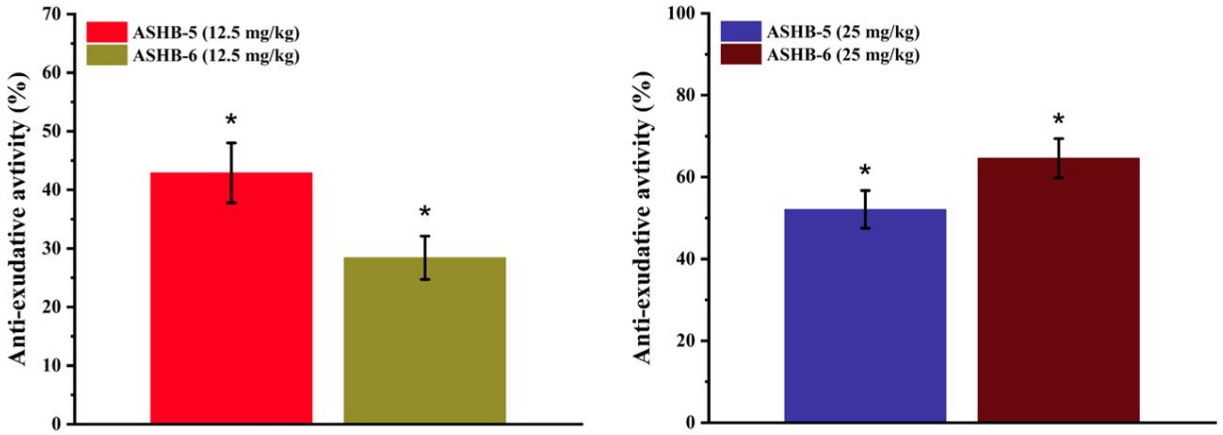


Figure 3 Anti-exudative activity of ASHB-5 and ASHB-6 at doses of 12.5 and 25 mg/kg, calculated at the 3rd h after carrageenan administration. Values are presented as mean ± SEM. Statistical significance is indicated as $*p < 0.05$ versus control.

Increasing the dose to 25 mg/kg resulted in a marked enhancement of the anti-exudative effects of both ASHB complexes. At this dose, ASHB-5 produced an anti-exudative activity of 52.1 ± 4.6% (**Figure 3**), exceeding its activity observed at 12.5 mg/kg. ASHB-6 exhibited a still stronger inhibitory effect, with anti-exudative activity reaching 64.6 ± 4.8%. These results indicate that dose elevation improved the anti-inflammatory efficacy of both ASHB-5 and ASHB-6. Interestingly, the activity pattern changed at the higher dose. While ASHB-5 was more effective than ASHB-6 at 12.5 mg/kg, ASHB-6 became the more active compound at 25 mg/kg. Its higher anti-exudative activity suggests that ASHB-6 may demonstrate a stronger dose-dependent response and may more effectively inhibit exudative edema formation during the peak stage of carrageenan-induced inflammation. Comparison of the 2 tested doses confirms a dose-related increase in anti-exudative activity for both complexes. The strongest effect was recorded for ASHB-6 at 25 mg/kg, supporting its greater potential to suppress mediator-driven inflammatory edema under the conditions of this experimental model.

Molecular docking insights into the anti-inflammatory potential of ASHB-5 and ASHB-6

The molecular docking targets were selected according to their functional importance in acute inflammation and their close association with the mechanisms involved in carrageenan-induced paw edema. In this study, COX-2, IL-6, MAPK, and NF-kB were used as key inflammation-related targets because each of them represents a distinct regulatory level of the inflammatory cascade. These proteins are involved in prostaglandin biosynthesis, cytokine-mediated inflammatory signaling, intracellular signal transmission, and transcriptional control of inflammatory mediator expression [14]. Therefore, this group of targets provided a biologically relevant basis for interpreting the possible molecular mechanisms through which ASHB-5 and ASHB-6 may exert the anti-inflammatory and anti-exudative effects observed *in vivo*.

COX-2 was chosen because it is one of the principal inducible enzymes activated during inflammation. It catalyzes the conversion of arachidonic acid into prostaglandins, especially prostaglandin E_2, which plays an important role in edema formation, vasodilation, increased vascular permeability, pain, and fever [15]. Since the later stage of carrageenan-induced paw edema is strongly dependent on prostaglandin production, predicted interactions of ASHB-5 and ASHB-6 with COX-2 may indicate their possible involvement in suppressing prostaglandin-associated inflammatory swelling.

IL-6 was selected as a major pro-inflammatory cytokine that contributes to the progression and maintenance of inflammatory responses. It is involved in immune cell activation, acute-phase reactions, and the coordination of local and systemic inflammatory

processes [16]. Because excessive IL-6 activity is associated with prolonged inflammatory signaling, docking studies with this target were performed to evaluate whether ASHB-5 and ASHB-6 could potentially interact with cytokine-related inflammatory mechanisms.

MAPK was included as an important intracellular signaling target because MAPK pathways are rapidly activated by inflammatory stimuli and participate in the regulation of cytokine production, mediator release, and cellular stress responses. These pathways transfer inflammatory signals from the cell surface to the nucleus and promote the activation of downstream genes involved in inflammation [17]. Thus, possible binding of ASHB-5 and ASHB-6 to MAPK may suggest a potential role in the modulation of intracellular inflammatory signaling.

NF-kB was selected due to its central role as a transcriptional regulator of inflammation. Upon activation, NF-kB promotes the expression of numerous inflammatory genes, including those encoding cytokines, chemokines, adhesion molecules, inducible nitric oxide synthase, and COX-2 [18]. Because NF-kB links upstream inflammatory stimuli with downstream gene expression, it represents a critical molecular target for evaluating the potential anti-inflammatory mechanisms of the investigated ASHB complexes.

Overall, the selected target panel covers several complementary components of the inflammatory process. COX-2 represents the enzymatic pathway responsible for prostaglandin generation, IL-6 reflects cytokine-driven inflammatory communication, MAPK represents intracellular signal transduction, and NF-kB reflects transcriptional regulation of inflammatory gene expression [19]. Docking ASHB-5 and ASHB-6 against these proteins therefore allowed a multi-target assessment of their possible mechanisms of action.

Since ASHB-5 and ASHB-6 are complex compounds, molecular docking was used to compare their predicted interaction profiles with the selected inflammatory targets. The analysis included binding energy values, estimated inhibition constants, and the types of ligand–protein contacts formed within the binding regions. More favorable binding energy, lower predicted Ki values, and stable non-covalent interactions with functionally important amino acid residues were considered indicators of stronger predicted target affinity [20]. It should be noted that docking-derived results provide theoretical and predictive information rather than direct experimental evidence of protein inhibition. For this reason, the molecular docking data were used as complementary mechanistic support for the *in vivo* findings. This approach helped to connect the experimentally observed anti-exudative effects of ASHB-5 and ASHB-6 with their possible interactions with key inflammation-associated molecular targets.

COX-2

The binding interaction between ASHB-5 and COX-2 was investigated using the predefined docking grid centered at x = 36.323000, y = 26.465000, and z = 23.686000 (**Figure 4**). As ASHB-5 represents a complex compound, its individual components were docked separately to evaluate their specific binding contributions within the COX-2 binding site. Both components displayed favorable interaction profiles with COX-2, yielding binding free energies of −8.3 and −9.4 kcal/mol. These negative energy values suggest stable ligand–receptor complex formation and indicate a favorable predicted affinity of ASHB-5 components toward the COX-2 target. Based on the obtained binding energy values, the predicted inhibition constants were estimated as approximately 0.824 μM for the component with ΔG = −8.3 kcal/mol and 0.129 μM for the component with ΔG = −9.4 kcal/mol (**Table 2**). The markedly lower Ki value of the latter component reflects stronger theoretical affinity for COX-2 and suggests that this part of the ASHB-5 complex may contribute more prominently to its potential COX-2-associated anti-inflammatory effect.

Table 2 Molecular docking binding energies and estimated Ki values of ASHB compounds against COX-2.

Ligands	Binding energy (Kcal/mol)	Estimated Ki value (μM)
ASHB-5	−8.3	0.824
	−9.4	0.129
ASHB-6	−7.8	1.91
	−9.6	091

Two-dimensional interaction mapping revealed that the first ASHB-5 component established multiple stabilizing contacts with COX-2 amino acid residues, including SER A:49, GLY A:135, ASN A:34, TYR A:130, PRO A:153, and TYR A:136. The interaction pattern involved conventional hydrogen bonds, carbon–hydrogen bonds, π-donor hydrogen bonds, π–π T-shaped contacts, alkyl interactions, and π–alkyl interactions. These non-covalent contacts may support stable accommodation of the ligand within the COX-2 binding pocket. The second component of ASHB-5 also exhibited a favorable binding pattern within COX-2, interacting with residues such as CYS A:47, GLN B:327, TYR A:134, ASP A:133, ALA A:132, and ASP A:157. This interaction profile was mainly supported by conventional hydrogen bonds and carbon–hydrogen bonds, indicating that hydrogen-bond formation may be an important factor in stabilizing this component in the receptor binding region.

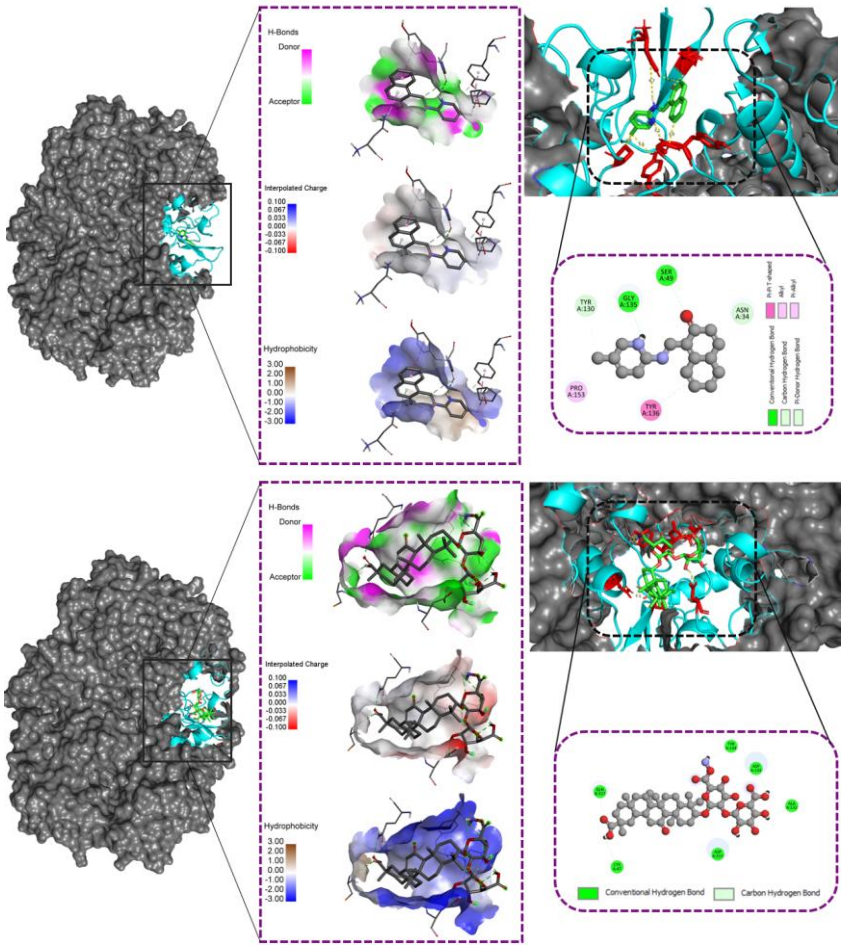


Figure 4 Molecular docking visualization of ASHB-5 within the COX-2 binding region. The figure shows the predicted binding pose of ASHB-5 in the COX-2 pocket, including 3D ligand–receptor orientation, hydrogen-bond donor/acceptor surface, interpolated charge distribution, hydrophobicity mapping, and 2D ligand–protein interaction profile.

The docking behavior of ASHB-6 against COX-2 was assessed using the same predefined grid parameters, with the grid center set at x = 36.323000, y = 26.465000, and z = 23.686000 (**Figure 4**). Because ASHB-6 is a complex compound, its structural components were docked independently to determine their individual binding contributions within the selected COX-2 binding region. Both components showed favorable predicted interactions with COX-2, producing binding free energy values of −7.8 and −9.6 kcal/mol. These negative docking energy values indicate energetically favorable ligand–receptor complex formation and suggest that ASHB-6 may interact effectively with the COX-2 target. The Ki values estimated from the corresponding binding energies were approximately 1.91 μM for the component with ΔG = −7.8 kcal/mol and 0.091 μM for the component with ΔG = −9.6 kcal/mol (**Table 2**). The lower predicted Ki value of the second component indicates a stronger theoretical affinity for the COX-2 binding site. This finding suggests that this component of the ASHB-6 complex may be more actively involved in the potential COX-2-related anti-inflammatory mechanism. Two-dimensional interaction analysis revealed that one ASHB-6 component established multiple non-covalent contacts with COX-2 amino acid residues, including ASN B:382, HIS B:386, HIS B:388, HIS B:207, ALA B:202, GLN B:203, and LEU B:391. The interaction profile consisted of conventional hydrogen bonds, π-associated contacts, π–alkyl interactions, π–sulfur interaction, and other stabilizing non-covalent forces. These contacts may contribute to stable ligand accommodation within the COX-2 binding pocket.

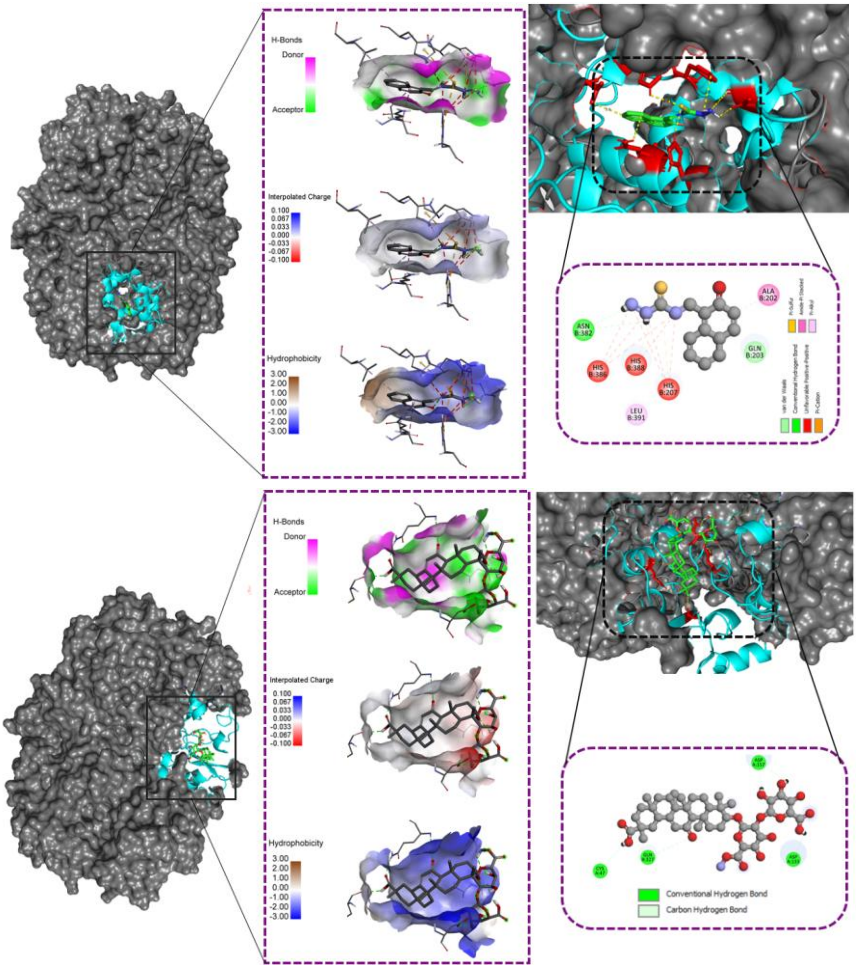


Figure 5 Molecular docking visualization of ASHB-6 within the COX-2 binding region. The figure shows the predicted binding pose of ASHB-6 in the COX-2 pocket, including 3D ligand–receptor orientation, hydrogen-bond donor/acceptor surface, interpolated charge distribution, hydrophobicity mapping, and 2D ligand–protein interaction profile.

The second ASHB-6 component also exhibited a favorable interaction pattern with COX-2, involving residues such as CYS A:47, GLN B:327, ASP A:157, and ASP A:133 (**Figure 5**). This binding profile was mainly characterized by conventional hydrogen bonds and carbon–hydrogen bonds, indicating that hydrogen-bonding interactions may play an important role in stabilizing this component within the receptor binding region.

IL-6

Following the COX-2 docking analysis, IL-6 was selected as the next inflammatory target because of its central role in pro-inflammatory signaling and immune response regulation. Docking simulations were carried out using the predefined IL-6 grid center coordinates x = −45.351000, y = 180.123000, and z = 40.952000. Since the ASHB samples are complex in nature, their individual structural components were docked separately to assess their specific binding behavior within the selected IL-6 binding region. The separated ASHB-5 components showed favorable predicted interactions with IL-6, with binding free energy values of −7.6 and −8.6 kcal/mol. These negative docking scores indicate energetically stable ligand–protein complex formation and suggest potential affinity of the investigated components toward the IL-6 target. Based on these binding energies, the predicted Ki values were estimated as approximately 2.68 μM for the component with ΔG = −7.6 kcal/mol and 0.496 μM for the component with ΔG = −8.6 kcal/mol. The lower Ki value of the latter component indicates stronger theoretical affinity for IL-6 (**Table 3**).

Table 3 Molecular docking binding energies and estimated Ki values of ASHB compounds against IL-6.

Ligands	Binding energy (Kcal/mol)	Estimated Ki value (μM)
ASHB-5	−7.6	2.68
	−8.6	0.496
ASHB-6	−6.3	24
	−8.3	0.824

The 2D interaction profile revealed that one docked component established several stabilizing contacts with IL-6 amino acid residues, including LEU B:57, PHE C:168, PHE C:134, ARG B:168, LYS B:66, and LEU B:165 (**Figure 6**). These interactions included conventional hydrogen bonding, π-cation interaction, π-sigma contact, alkyl interaction, π–alkyl interaction, and one unfavorable positive–positive contact. The combination of hydrogen-bonding and hydrophobic interactions suggests that this component may be stabilized within the IL-6 binding region through multiple non-covalent forces. The second docked component displayed a broader interaction network dominated by hydrogen bonding. It interacted with IL-6 residues including ARG C:233, TRP C:284, LYS B:54, SER B:52, GLY C:282, GLY C:193, ARG B:40, and GLY C:280. The interaction pattern was mainly represented by conventional hydrogen bonds and carbon–hydrogen bonds, indicating that hydrogen-bond formation may be a key contributor to the stabilization of this component within the IL-6 binding site.

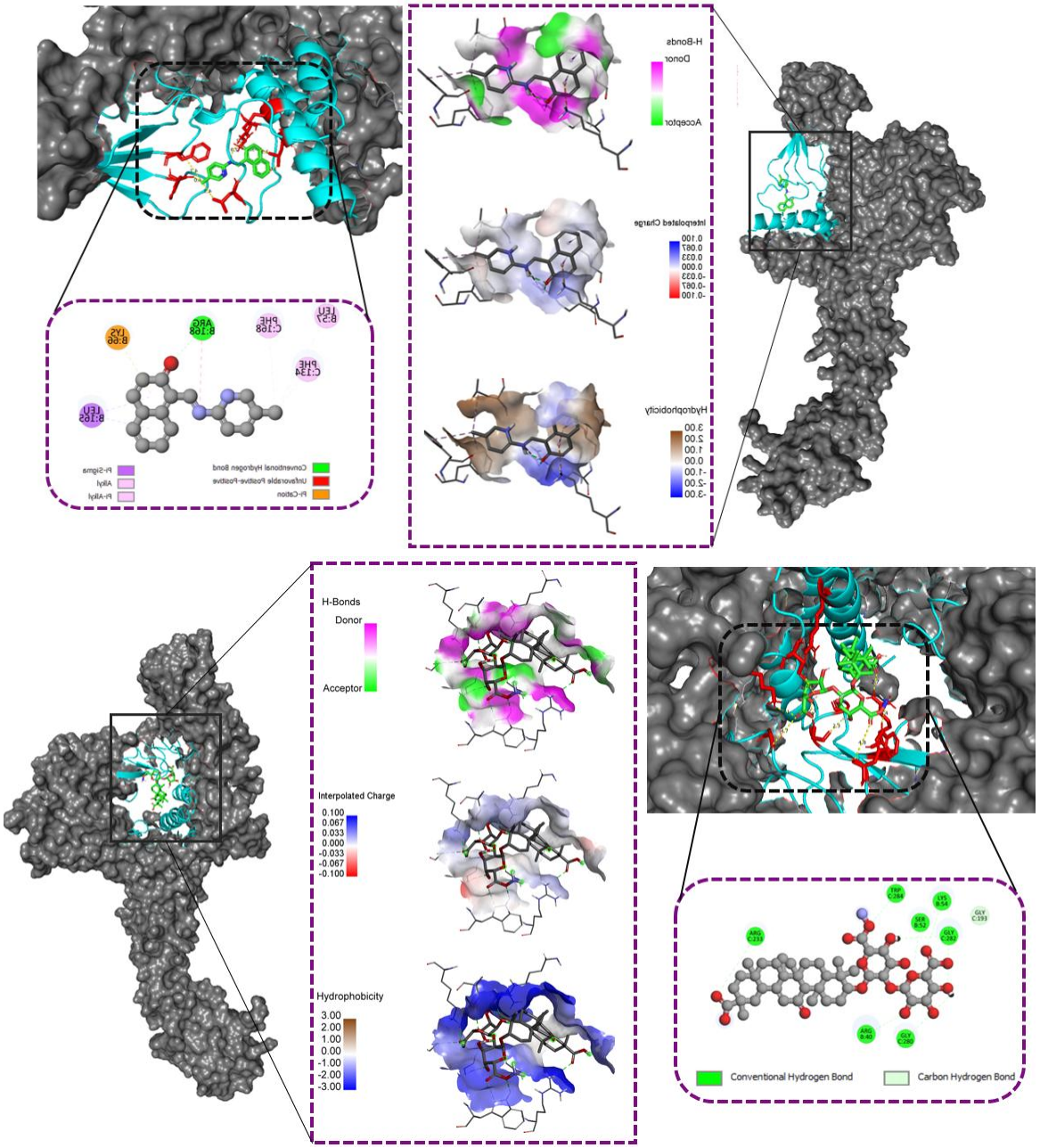


Figure 6 Molecular docking visualization of ASHB-5 components within the IL-6 binding region. The figure shows the predicted binding pose, ligand–protein orientation, hydrogen-bond donor/acceptor surface, interpolated charge distribution, hydrophobicity map, and 2D interaction profile of ASHB-5 components docked with IL-6.

The second docked component displayed a broader interaction network dominated by hydrogen bonding. It interacted with IL-6 residues including ARG C:233, TRP C:284, LYS B:54, SER B:52, GLY C:282, GLY C:193, ARG B:40, and GLY C:280. The interaction pattern was mainly represented by conventional hydrogen bonds and carbon–hydrogen bonds, indicating that hydrogen-bond formation may be a key contributor to the stabilization of this component within the IL-6 binding site. After evaluating the interaction of ASHB-5 with IL-6, ASHB-6 was also subjected to docking analysis using the same predefined IL-6 grid center coordinates: x = −45.351000, y = 180.123000, and z = 40.952000. Since ASHB-6 is a complex compound, its individual components were docked separately to assess their specific binding behavior within the selected IL-6 binding region.

The docking results demonstrated that the separated components of ASHB-6 were able to form favorable interactions with IL-6, showing binding free

energy values of −6.3 and −8.3 kcal/mol. Although both values indicate energetically favorable ligand–protein binding, the interaction strength was not equal between the 2 components. The predicted Ki values derived from these binding energies were approximately 24.0 μM for the component with ΔG = −6.3 kcal/mol and 0.824 μM for the component with ΔG = −8.3 kcal/mol (**Table 3**). The considerably lower Ki value of the second component indicates stronger theoretical affinity toward IL-6, suggesting that this structural part of ASHB-6 may be more relevant to its potential cytokine-associated anti-inflammatory effect. The 2D interaction map of the first ASHB-6 component revealed contacts with IL-6 residues, including HIS A:145, LYS B:120, VAL B:121, and neighboring amino acid residues (**Figure 6**). The interaction profile involved carbon–hydrogen bonds, π–π stacked interactions, π–alkyl contacts, π-cation interaction, and one unfavorable positive–positive interaction. These findings suggest that aromatic and hydrophobic contacts may contribute to the stabilization of this component within the IL-6 binding region.

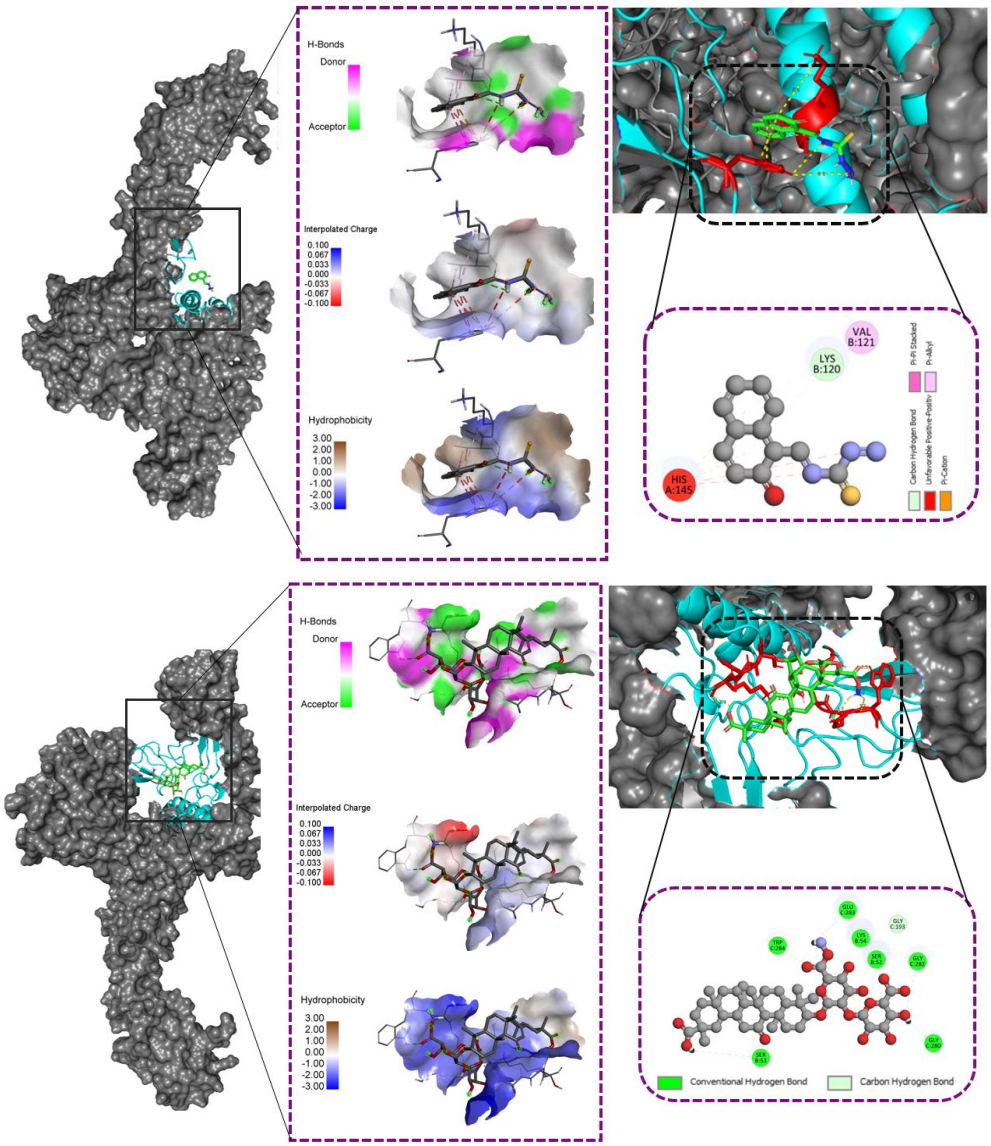


Figure 7 IL-6 andASHB-6 docking complex: binding orientation and interaction mapping.

The second ASHB-6 component displayed a broader interaction network, mainly supported by hydrogen-bonding contacts. This component interacted with several IL-6 residues, including SER B:53, TRP C:284, GLU C:283, LYS B:54, SER B:52, GLY C:193, GLY C:282, and GLY C:280 (**Figure 7**). The presence of conventional hydrogen bonds and carbon–hydrogen bonds indicates that hydrogen-bond formation may play a major role in maintaining the stability of this ligand within the IL-6 binding pocket. When compared with ASHB-5, which produced IL-6 binding energies of −7.6 and −8.6 kcal/mol, ASHB-6 showed a slightly weaker overall interaction profile, especially for the component with ΔG = −6.3 kcal/mol. Nevertheless, the second ASHB-6 component, with ΔG = −8.3 kcal/mol and an estimated Ki value of 0.824 μM, still demonstrated favorable predicted binding toward IL-6. These results indicate that ASHB-6 may also interact with IL-6, although its predicted cytokine-related affinity appears somewhat lower than that of ASHB-5 under the same docking conditions.

MAPK

After the docking studies with COX-2 and IL-6, ASHB-5 was additionally assessed against MAPK, a key intracellular signaling protein involved in the regulation of inflammatory mediator production. The docking procedure was carried out using the defined MAPK grid center coordinates x = 3.247000, y = 17.679000, and z = 31.593000. Because ASHB-5 is a complex compound, its structural components were docked individually to evaluate their separate binding contributions within the selected MAPK binding region. The separated ASHB-5 components showed favorable predicted interactions with MAPK, with binding free energy values of −6.9 and −8.0 kcal/mol.

Table 4 Molecular docking binding energies and estimated Ki values of ASHB compounds against MAPK.

Ligands	Binding energy (Kcal/mol)	Estimated Ki value (μM)
ASHB-5	−6.9	8.75
	−8.0	1.35
ASHB-6	−6.4	20.2
	−8.6	0.496

Although both values indicate energetically favorable ligand–protein binding, the second component demonstrated stronger interaction. The estimated Ki values derived from these energies were approximately 8.75 μM for the component with ΔG = −6.9 kcal/mol and 1.35 μM for the component with ΔG = −8.0 kcal/mol. The lower Ki value of the latter component indicates a higher theoretical affinity toward the MAPK binding site. The 2D interaction profile of the first ASHB-5 component showed contacts with several MAPK residues, including PRO A:350, ASP A:88, THR A:91, ILE A:346, and ARG A:5. These interactions involved conventional hydrogen bonding, π–alkyl interactions, and other stabilizing non-covalent contacts, which may support ligand stabilization within the MAPK binding pocket.

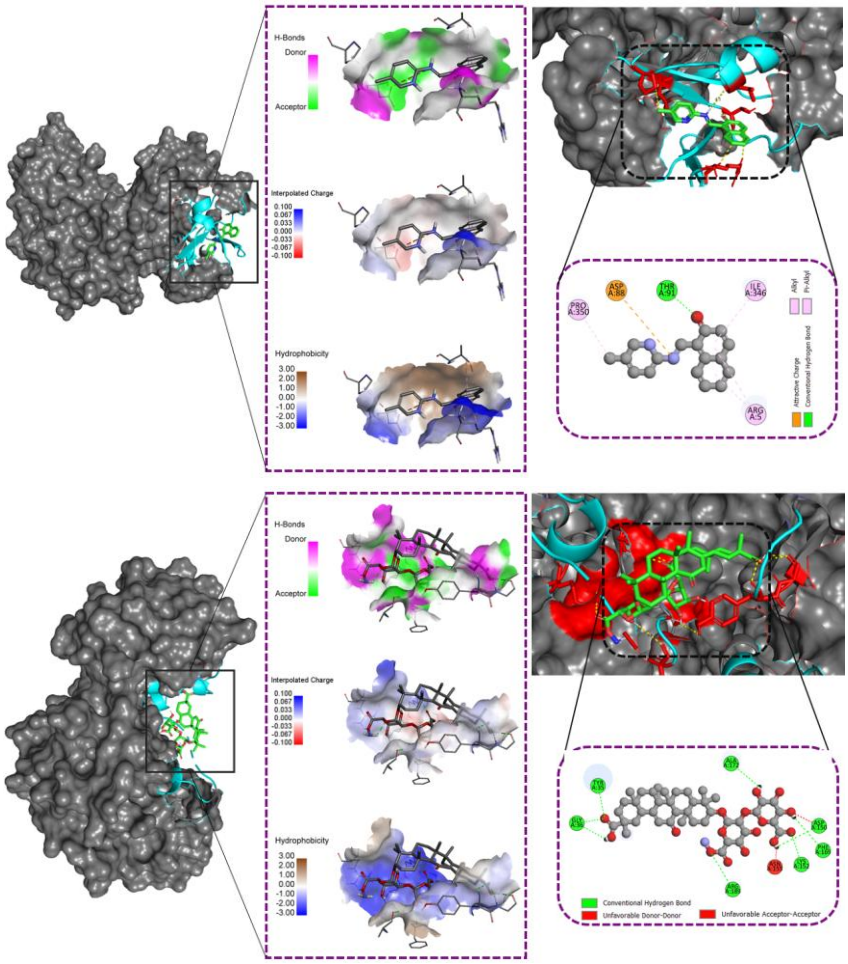


Figure 8 MAPK–ASHB-5 docking complex: binding orientation and interaction mapping.

The second ASHB-5 component displayed a wider interaction network within the MAPK binding region. It interacted with residues such as TYR A:35, GLY A:36, ALA A:172, ASP A:150, ASN A:155, LYS A:152, PHE A:169, and ARG A:189 (**Figure 8**). This interaction pattern was mainly supported by hydrogen bonds and additional stabilizing contacts, suggesting that polar interactions may contribute importantly to maintaining ligand stability in the receptor binding site. Compared with its stronger predicted interactions with COX-2 and IL-6, ASHB-5 exhibited a moderate but still favorable binding profile toward MAPK. Among the 2 docked components, the structure with ΔG = −8.0 kcal/mol and an estimated Ki value of 1.35 μM showed the better interaction profile. Since MAPK participates in intracellular inflammatory signal transduction and cytokine expression regulation, these docking findings suggest that ASHB-5 may also contribute to anti-inflammatory activity through possible interaction with MAPK-associated signaling pathways.

After completing the MAPK docking assessment for ASHB-5, ASHB-6 was analyzed under the same docking conditions using the grid center coordinates x = 3.247000, y = 17.679000, and z = 31.593000. Because ASHB-6 is a complex compound, its structural components were docked individually to evaluate their separate binding contributions within the selected MAPK binding region. The separated ASHB-6 components showed favorable predicted binding toward MAPK, with binding free energy values of −6.4 and −8.6 kcal/mol (**Table 4**). Although both values suggest energetically favorable ligand–protein complex formation, the component with ΔG = −8.6 kcal/mol exhibited a considerably stronger binding profile. The estimated Ki values derived from these docking energies were approximately 20.2 μM and 0.496 μM, respectively. The lower Ki value of the second

component indicates higher theoretical affinity for the MAPK binding site. The first ASHB-6 component interacted with several MAPK residues, including ARG A:5, ASP A:88, VAL A:89, THR A:91, VAL A:345, and ILE A:346 (**Figure 9**).

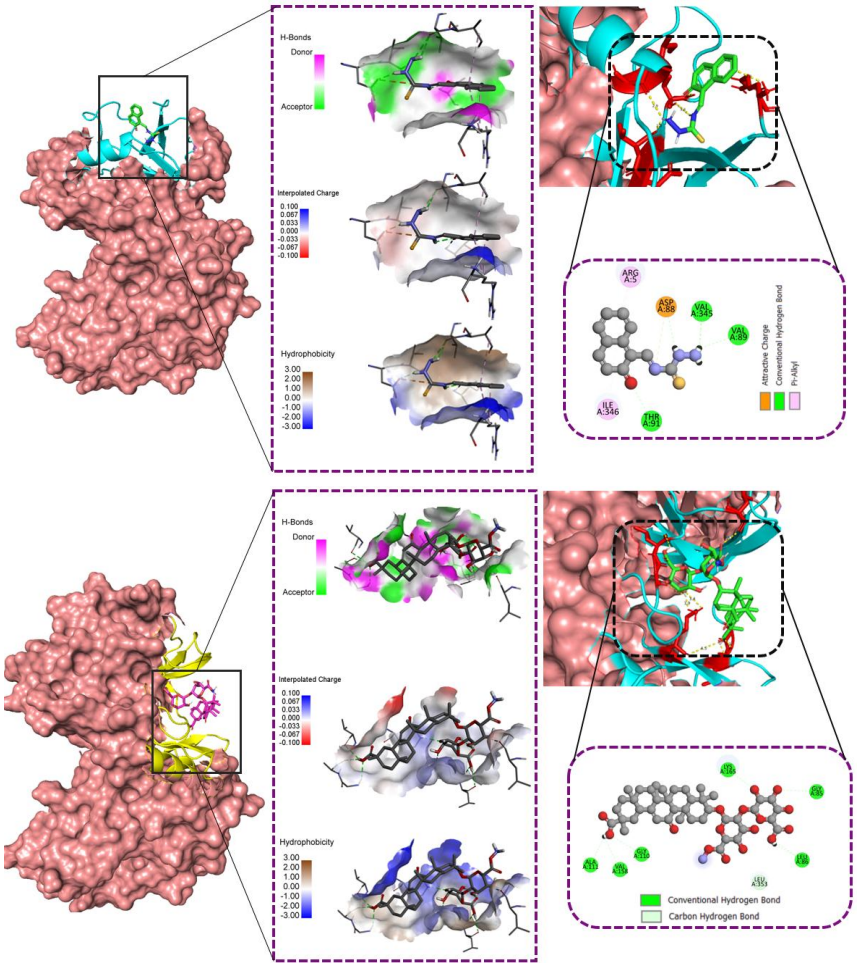


Figure 9 MAPK–ASHB-6 docking complex: binding orientation and interaction mappin.

The interaction pattern involved conventional hydrogen bonds, attractive charge interaction, and π–alkyl contacts. These non-covalent interactions may support the stabilization of this component within the MAPK binding pocket. The second ASHB-6 component displayed a wider interaction network involving ALA A:111, GLY A:110, VAL A:158, LYS A:165, GLY A:85, LEU A:86, and LEU A:353 (**Figure 9**). Its binding profile was mainly characterized by conventional hydrogen bonds and carbon–hydrogen bonds, suggesting that hydrogen-bonding interactions may be important for maintaining ligand stability within the MAPK binding region. Compared with ASHB-5, which showed MAPK binding energies of −6.9 and −8.0 kcal/mol, ASHB-6 demonstrated a stronger best binding score, particularly for the component with ΔG = −8.6 kcal/mol. This indicates that ASHB-6 may have a more favorable predicted interaction with MAPK. Since MAPK plays an important role in intracellular inflammatory signal transduction and cytokine expression, these docking findings suggest that ASHB-6 may contribute to anti-inflammatory activity through possible modulation of MAPK-associated signaling pathways.

NF-kB

NF-kB was included in the docking study as a key transcriptional regulator involved in the control of inflammation-related gene expression. The docking simulation was carried out in the selected NF-kB

binding region using the grid center coordinates x = 27.659000, y = 19.514000, and z = 36.394000. Because ASHB-5 is a complex compound, its structural components were docked independently to assess their separate binding behavior and interaction profiles with the NF-kB target.

Table 5 Molecular docking binding energies and estimated Ki values of ASHB compounds against NF-kB.

Ligands	Binding energy (Kcal/mol)	Estimated Ki value (μM)
ASHB-5	−9.1	0.213
	−9.2	0.18
ASHB-6	−7.7	2.27
	−10.4	0.024

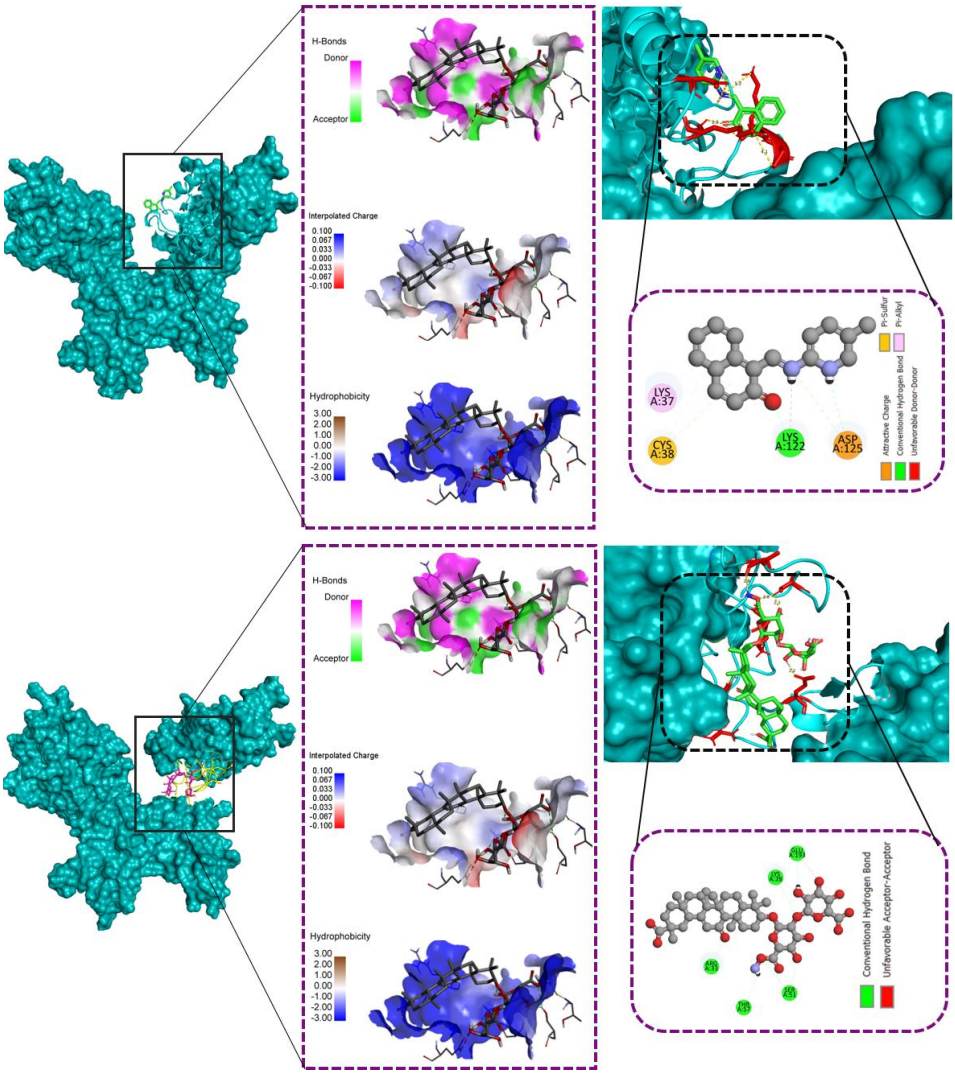
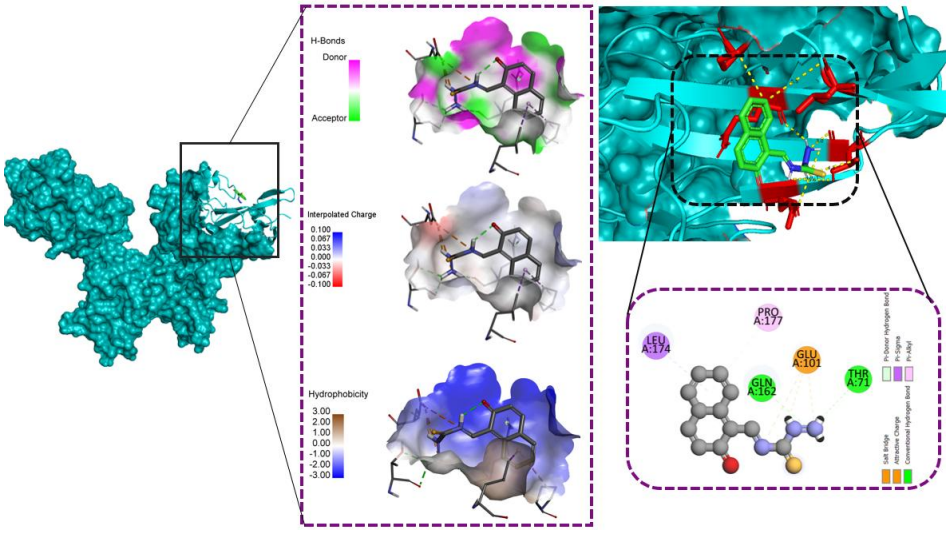


Figure 10 NF-kB binding pattern of ASHB-5 components revealed by molecular docking.

The obtained docking results indicated that both ASHB-5 components exhibited strong predicted affinity toward NF-kB, with binding free energy values of −9.1 and −9.2 kcal/mol. These highly negative values reflect energetically favorable ligand–protein complex formation and suggest stable accommodation of ASHB-5 components within the NF-kB binding region. The corresponding estimated Ki values were approximately 0.213 μM for the component with ΔG = −9.1 kcal/mol and 0.180 μM for the component with ΔG = −9.2 kcal/mol (**Table 5**). The lower Ki value of the latter component indicates slightly stronger theoretical affinity for NF-kB. The 2D interaction map of the first ASHB-5 component showed contacts with several NF-kB amino acid residues, including LYS A:37, CYS A:38, LYS A:122, and ASP A:125. The interaction network consisted of conventional hydrogen bonds, attractive charge interaction, π–sulfur interaction, π–alkyl contacts, and one unfavorable donor–donor contact. These findings suggest that electrostatic forces, hydrophobic interactions, and hydrogen bonding may jointly contribute to ligand stabilization within the NF-kB binding site.

The second ASHB-5 component also displayed a favorable binding pattern with NF-kB. It interacted with ARG A:33, LYS A:28, GLU A:193, SER A:51, and THR A:57 (**Figure 10**). This interaction profile was mainly supported by conventional hydrogen bonds, indicating that hydrogen-bond formation may be one of the main stabilizing factors for this component in the receptor binding region. Although an unfavorable acceptor–acceptor interaction was detected with GLU A:193, the overall docking energy remained strongly favorable.

After the NF-kB docking analysis of ASHB-5, ASHB-6 was examined under the same docking conditions using the predefined grid center coordinates x = 27.659000, y = 19.514000, and z = 36.394000. Because ASHB-6 is a complex compound, its structural components were docked individually to evaluate their separate binding contributions within the selected NF-kB binding region. The separated ASHB-6 components showed favorable predicted binding with NF-kB, producing binding free energy values of −7.7 and −10.4 kcal/mol. Although both values indicate energetically favorable ligand–protein complex formation, the component with ΔG = −10.4 kcal/mol displayed a notably stronger binding profile. The corresponding estimated Ki values were approximately 2.27 μM and 0.024 μM, respectively (**Table 5**). The markedly lower Ki value of the second component indicates high theoretical affinity toward the NF-kB binding region. The first ASHB-6 component interacted with several NF-kB residues, including LEU A:174, PRO A:177, GLN A:162, GLU A:101, and THR A:71. Its interaction pattern involved conventional hydrogen bonds, salt bridge interaction, attractive charge contacts, π-donor hydrogen bonding, π-sigma interaction, and π–alkyl contacts. These interactions suggest that electrostatic forces, hydrogen bonding, and hydrophobic contacts may collectively support ligand stabilization within the NF-kB binding pocket.



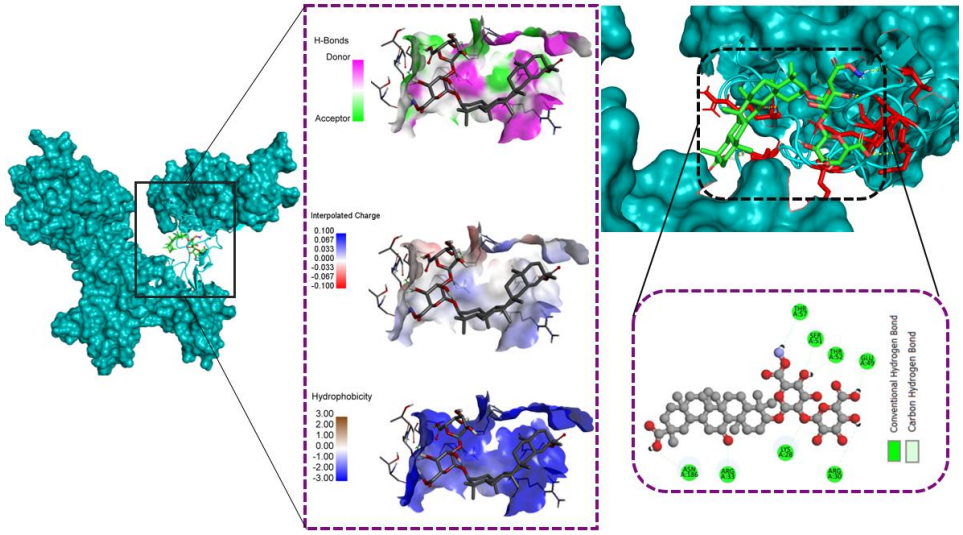


Figure 11 NF-kB binding pattern of ASHB-6 components revealed by molecular docking.

The second ASHB-6 component established a wider interaction network dominated by hydrogen-bonding contacts. It interacted with ASN A:186, ARG A:33, LYS A:28, THR A:57, SER A:51, THR A:52, GLU A:49, and ARG A:30 (**Figure 11**). The presence of conventional hydrogen bonds and carbon–hydrogen bonds indicates that hydrogen-bond formation may be one of the main factors responsible for stabilizing this component within the receptor binding site. Compared with ASHB-5, which showed NF-kB binding energies of −9.1 and −9.2 kcal/mol, ASHB-6 demonstrated a stronger best docking result, especially for the component with ΔG = −10.4 kcal/mol. This suggests that ASHB-6 may interact more favorably with NF-kB than ASHB-5 under the same docking conditions. Since NF-kB regulates the transcription of many inflammatory mediators, including cytokines, chemokines, iNOS, and COX-2, the strong predicted binding profile of ASHB-6 may support its pronounced anti-exudative activity observed in the carrageenan-induced paw edema model.

Discussion

This study evaluated the anti-inflammatory potential of ASHB-5 and ASHB-6 complexes using integrated *in vivo* and *in silico* approaches. In the carrageenan-induced paw edema model, both complexes reduced acute exudative inflammation in rats. In the untreated control group, paw edema increased progressively and reached its maximum at the 3rd h after carrageenan administration, with a value of 73.9 ± 7.2%. Therefore, this time point was considered the peak phase of inflammation and was used to assess anti-exudative activity. At 12.5 mg/kg, ASHB-5 showed stronger anti-exudative activity than ASHB-6, producing 42.9 ± 5.1% inhibition compared with 28.4 ± 3.7% for ASHB-6. However, at 25 mg/kg, the activity pattern changed. ASHB-5 showed 52.1 ± 4.6% anti-exudative activity, whereas ASHB-6 produced the strongest effect, reaching 64.6 ± 4.8%. These findings indicate a dose-dependent enhancement of anti-inflammatory activity for both complexes, with ASHB-6 being more effective at the higher dose. The strong inhibition observed at the 3rd h suggests that ASHB-5 and ASHB-6 may affect the late phase of carrageenan-induced inflammation, which is mainly associated with prostaglandin production, COX-2 activation, cytokine release, and inflammatory gene regulation. This indicates that the tested complexes may suppress mediator-dependent inflammatory mechanisms rather than only influencing the early vascular phase of inflammation.

The molecular docking analysis provided complementary computational evidence for potential interactions of ASHB-5 and ASHB-6 with COX-2, IL-6, MAPK, and NF-κB. However, these results represent predicted ligand–protein affinity and should not be interpreted as direct evidence of target inhibition or pathway modulation. Both complexes showed favorable predicted binding toward COX-2, with the best score observed for ASHB-6 (−9.6 kcal/mol). ASHB-5 showed slightly stronger predicted affinity toward IL-6, whereas ASHB-6 produced the most favorable MAPK score

(−8.6 kcal/mol). NF-κB showed the strongest overall predicted interaction, particularly with one ASHB-6 component, which yielded a binding energy of −10.4 kcal/mol and an estimated Ki of approximately 0.024 μM. These docking patterns may be considered alongside the observed *in vivo* anti-exudative effects, but they do not establish a causal mechanism. Therefore, COX-2, IL-6, MAPK, and NF-κB should be regarded as potential molecular targets requiring confirmation through enzyme inhibition assays, cytokine measurements, and pathway-specific experimental studies.

A limitation of the present study is the small number of animals included in each experimental group and the absence of an a priori power calculation. Accordingly, the *in vivo* findings should be interpreted as preliminary. Although repeated-measures analysis was applied to account for within-animal correlations over time, the limited sample size reduces statistical power and restricts the generalizability of the results. Further studies with larger groups and prospectively determined sample sizes are required to confirm the reproducibility and magnitude of the observed anti-exudative effects. Another limitation of the present study is the absence of a standard anti-inflammatory drug as a positive control. Therefore, the relative pharmacological potency of ASHB-5 and ASHB-6 cannot be directly compared with that of established anti-inflammatory agents. Future studies should include an appropriate reference drug, such as indomethacin or diclofenac, to provide a more reliable benchmark for efficacy.

Overall, the combined *in vivo* and docking results suggest that ASHB-5 and ASHB-6 may act through multi-target anti-inflammatory mechanisms. ASHB-5 showed relatively favorable interaction with IL-6 and NF-kB and was more active at the lower dose. In contrast, ASHB-6 showed stronger docking results against COX-2, MAPK, and NF-kB and produced the highest anti-exudative activity at 25 mg/kg. This suggests that ASHB-6 may exert stronger activity through broader modulation of prostaglandin-dependent, intracellular signaling, and transcriptional inflammatory pathways. Since ASHB-5 and ASHB-6 are complex compounds, their biological effects may result from the combined contribution of several structural components. Docking was therefore useful for identifying components with stronger predicted binding affinity and stable non-covalent interactions. However, docking results should be interpreted as computational predictions rather than direct proof of target inhibition. Further studies, including COX-2 inhibition assays, cytokine measurements, Western blotting, and gene expression analysis, are needed to confirm the proposed mechanisms. In conclusion, ASHB-5 and ASHB-6 demonstrated promising anti-inflammatory and anti-exudative activity in the carrageenan-induced paw edema model. The *in vivo* effects were supported by molecular docking interactions with COX-2, IL-6, MAPK, and NF-kB. Among the tested complexes, ASHB-6 showed the strongest activity at 25 mg/kg and the most favorable docking profile against key inflammatory targets, particularly NF-kB and COX-2. These findings suggest that ASHB-6 may be a more potent anti-inflammatory candidate, while ASHB-5 also shows meaningful activity, especially at the lower dose.

Conclusions

The present study demonstrated that ASHB-5 and ASHB-6 complexes possess promising anti-inflammatory and anti-exudative activity in the carrageenan-induced paw edema model. Both complexes reduced paw edema formation compared with the untreated control group, confirming their ability to attenuate acute exudative inflammation. The anti-inflammatory effect was dose-dependent, as both ASHB-5 and ASHB-6 showed stronger activity at 25 mg/kg than at 12.5 mg/kg. At the lower dose of 12.5 mg/kg, ASHB-5 exhibited a stronger anti-exudative effect than ASHB-6, indicating its higher activity under low-dose conditions. In contrast, at 25 mg/kg, ASHB-6 produced the most pronounced inhibition of paw edema during the peak inflammatory phase, suggesting a stronger dose-responsive anti-inflammatory profile. These findings indicate that both complexes are active, but their efficacy differs depending on the administered dose. The molecular docking results supported the *in vivo* findings by showing favorable predicted interactions of ASHB-5 and ASHB-6 with key inflammation-related targets, including COX-2, IL-6, MAPK, and NF-kB. These targets are involved in prostaglandin formation, cytokine-mediated inflammation, intracellular signaling, and transcriptional regulation of inflammatory mediator

expression. Among the investigated targets, COX-2 and NF-kB showed particularly favorable docking profiles, especially for ASHB-6, which demonstrated the strongest binding interaction with NF-kB. Overall, the integrated *in vivo* and *in silico* results suggest that ASHB-5 and ASHB-6 may exert anti-inflammatory activity through multi-target mechanisms. The observed reduction in paw edema may be associated with modulation of prostaglandin-dependent inflammation, cytokine-related signaling, MAPK-associated intracellular pathways, and NF-kB-mediated transcriptional regulation. ASHB-6 appears to be the more potent complex at the higher tested dose, whereas ASHB-5 also demonstrated meaningful anti-exudative activity, particularly at the lower dose. These findings support further pharmacological investigation of ASHB-5 and ASHB-6 as potential multi-target anti-inflammatory candidates. However, the molecular docking results should be considered predictive and require experimental confirmation. Future studies involving COX-2 inhibition assays, cytokine measurements, MAPK/NF-kB pathway analysis, and additional pharmacological safety evaluation are needed to confirm the proposed mechanisms of action and therapeutic potential of these complexes.

Acknowledgments

We have no grant and we also would like to thanks for Namangan State University in Uzbekistan for their great contributions. The research was carried out using institutional resources of the Namangan State University of the Republic of Uzbekistan.

Declaration of competing interest

The authors declare that they have no known competing financial interests or personal relationships that could have appeared to influence the work reported in this paper.

Declaration of generative AI in scientific writing

The authors acknowledge the use of generative AI tools for language editing and grammar correction. No content generation or data interpretation was performed by AI. The authors take full responsibility for the content and conclusions of this work.

CRediT author statement

Bakiyeva Muazzam: Conceptualization, Supervision, Project Administration, writing - Review & Editing. **Dadamirzayeva Kamola**, **Rezhepov Kural Zhedgerovich**: Investigation, Methodology, Data Curation, Formal Analysis, Writing - Original Draft, Methodology, Laboratory Experiments, Data Collection. **Najimov Akmaljon**, **Shiyrin Bekniyaz Kizi Alimbayeva.**, **Bekniyaz Alimbayevich Khodzhaniyazov.**: Validation, Resources, Experimental Design.

Reference

[1] MS Bakieva, SR Rustamova, TO Rakhmonov, NN Sharipova and KS Mukhitdinova. Hypotensive effect of the alkaloid benzoylheteratisine on the functional activity of rat aortic smooth muscle cells. *Academic Research Journal* 2022; **1(2)**, 24-30.

[2] W Li, LN Tu, L Hsieh, JR Smith, YT Yeh, A Sinyagin, EGB Evans, M Ghassemian, A Timms, K Charette, D Mauchley, M McMullan, L Bohuta, C Greene, MC Regier, JCD Alamo, R Savan and V Nigam. A shear stress-responsive pathway in monocytes drives cardiopulmonary bypass-induced inflammation via spectrin/RAF1/store-operated calcium entry. *Cell Reports* 2026; **45(2)**, 116903.

[3] HMH Martinez, E Barragan, KO Marichev, D Chávez-Flores and A Bugarin. Phthalimides as anti-inflammatory agents. *Future Medicinal Chemistry* 2025; **17(1)**, 125-142.

[4] MT Labro. Antibiotics as anti-inflammatory agents. *Current Opinion in Investigational Drugs* 2002; **3(1)**, 61-68.

[5] SS Adams and R Cobb. Non-steroidal anti-inflammatory drugs. *Progress in Medicinal Chemistry* 1967; **5**, 59-138.

[6] DR Royall and RF Palmer. INFLAMMATION's cognitive impact revealed by a novel “Line of Identity” approach. *PLoS One* 2024; **19(3)**, e0295386.

[7] T Li, R Guo, Q Zong and G Ling. Application of molecular docking in elaborating molecular mechanisms and interactions of supramolecular cyclodextrin. *Carbohydrate Polymers* 2022; **276**, 118644.

[8] X Liu, F Zhu, XH Ma, Z Shi, SY Yang, YQ Wei and YZ Chen. Predicting targeted polypharmacology for drug repositioning and multi-target drug discovery. *Current Medicinal Chemistry* 2013; **20(13)**, 1646-1661.

[9] Z Fang, H Ran, Y Zhang, C Chen, P Lin, X Zhang and M Wu. AlphaFold 3: An unprecedented opportunity for fundamental research and drug development. *Precision Clinical Medicine* 2025; **8(3)**, pbaf015.

[10] LG Ferreira, RN Dos Santos, G Oliva and AD Andricopulo. Molecular docking and structure-based drug design strategies. *Molecules* 2015; **20(7)**, 13384-13421.

[11] B Kaur and P Singh. Inflammation: Biochemistry, cellular targets, anti-inflammatory agents and challenges with special emphasis on cyclooxygenase-2. *Bioorganic Chemistry* 2022; **121**, 105663.

[12] MDS Maia, GCS Rodrigues, ABS Cavalcanti, L Scotti and MT Scotti. Consensus analyses in molecular docking studies applied to medicinal chemistry. *Mini-Reviews in Medicinal Chemistry* 2020; **20(14)**, 1322-1340.

[13] MD Ferrer, C Busquets-Cortés, X Capó, S Tejada, JA Tur, A Pons and A Sureda. Cyclooxygenase-2 inhibitors as a therapeutic target in inflammatory diseases. *Current Medicinal Chemistry* 2019; **26(18)**, 3225-3241.

[14] M Vasarri and D Degl'innocenti. Exploring marine-derived antioxidant and anti-inflammatory agents: Findings from recent studies. *Marine Drugs* 2025; **23(6)**, 240.

[15] H Wood. Anti-inflammatory drugs could cause chronic pain. *Nature Reviews Neurology* 2022; **18(7)**, 382.

[16] Redaktsiia. Clinical guidelines "Rational use of nonsteroidal anti-inflammatory drugs (NSAIDs) in clinical practice". Part I. *Zhurnal Nevrologii i Psikhiatrii imeni S.S. Korsakova* 2015; **115(4)**, 70-82.

[17] DV Tudor, I Bâldea, M Lupu, T Kacso, E Kutasi, A Hopârtean, R Stretea and AG Filip. COX-2 as a potential biomarker and therapeutic target in melanoma. *Cancer Biology & Medicine* 2020; **17(1)**, 20-31.

[18] YJ Guo, WW Pan, SB Liu, ZF Shen, Y Xu and LL Hu. ERK/MAPK signalling pathway and tumorigenesis. *Experimental and Therapeutic Medicine* 2020; **19(3)**, 1997-2007.

[19] EO Gubernatorova, EA Gorshkova, AI Polinova and MS Drutskaya. IL-6: Relevance for immunopathology of SARS-CoV-2. *Cytokine & Growth Factor Reviews* 2020; **53**, 13-24.

[20] NA El-Shitany and BG Eid. Icariin modulates carrageenan-induced acute inflammation through HO-1/Nrf2 and NF-kB signaling pathways. *Biomedicine & Pharmacotherapy* 2019; **120**, 109567.